energies

MDPI

Article

CFD Steady Model Applied to a Biomass Boiler Operating in Air Enrichment Conditions

Miguel Ángel Gómez [1,*], Rubén Martín [2], Joaquín Collazo [2] and Jacobo Porteiro [2]

[1] Defense University Center, Spanish Naval Academy, Plaza de España s/n 36900 Marín, Spain
[2] Industrial Engineering School, University of Vigo, Lagoas-Marcosende s/n 36310 Vigo, Spain; rubenmartinares@gmail.com (R.M.); joaquincollazo@uvigo.es (J.C.); porteiro@uvigo.es (J.P.)
* Correspondence: miguelgr@uvigo.es

Received: 15 August 2018; Accepted: 14 September 2018; Published: 21 September 2018



Abstract: A numerical model is proposed to perform CFD simulations of biomass boilers working in different operating conditions and analyse the results with low computational effort. The model is based on steady fluxes that represent the biomass thermal conversion stages through the conservation of mass, energy, and chemical species in the packed bed region. The conversion reactions are combined with heat and mass transfer submodels that release the combustion products to the gas flow. The gas flow is calculated through classical finite volume techniques to model the transport and reaction phenomena. The overall process is calculated in a steady state with a fast, efficient, and reasonably accurate method, which allows the results to converge without long computation times. The modelling is applied to the simulation of a 30 kW domestic boiler, and the results are compared with experimental tests with reasonably good results for such a simple model. The model is also applied to study the effect of air enrichment in boiler performance and gas emissions. The boiler operation is simulated using different oxygen concentrations that range from 21% to 90% in the feeding air, and parameters such as the heat transferred, fume temperatures, and emissions of CO, CO_2, and NO_x are analysed. The results show that with a moderated air enrichment of 40% oxygen, the energy performance can be increased by 8%, CO emissions are noticeably reduced, and NO_x remains practically stable.

Keywords: CFD modelling; biomass boiler; combustion; air enrichment

1. Introduction

The need to reduce the use of fossil fuels in the recent decades has led to the investigation of alternative fuels and combustion systems. This need produced a notorious increase in the interest in the use of biomass for energy production, especially for heat production. The development of efficient combustion systems such as biomass boilers and furnaces is a key factor to establish biomass as a reliable energy source. The development of computational technology has allowed for research of the combustion phenomena through simulation models, which provide the opportunity to analyse the behaviour of combustion systems easily and reduce costs [1,2]. Modelling a biomass boiler is a complex process that requires the combination of several models and techniques, and developing a reliable and efficient simulation model is still an important challenge. Numerous strategies have been proposed by studies. Some overviews on the modelling of biomass combustion were presented by Chaney et al. [3], Karin and Naser [4], and Khodaei et al. [5] presented in-depth reviews about different bed combustion approaches and submodels. CFD simulation codes are widely developed for the simulation of gaseous combustion. Yang et al. [6] studied the hydrodynamics within counter-current flow packed beds with and detailed meshing which gives a high accuracy of gas phase variables fields. However, the conversion of solid biomass is still a field in development. Therefore, the biomass bed is the critical zone

in the modelling of a combustion system. The simpler approach in the combustion of a biomass bed is to introduce the gases leaving the bed as a boundary condition in the boiler furnace. Eskilson et al. [7] used experimental measurements of these gases to define the properties of this inlet. Other works [8–11] calculate this boundary condition through the mass and energy balances, which aim to predict the results of the thermal conversion of solid biomass. Porteiro et al. [8] calculated the conversion of each incoming particle in the bed to generate the bed emissions. Previous works [9–11] have modelled the advance of biomass in a grate though several discrete columns whose properties change with the column position. All these works calculate the bed conversion out of the computational domain. A more accurate approach is to introduce the packed bed in the boiler CFD domain to use the local properties of each point in the conversion calculations through user defined functions (UDF). More complex models are those that meshed the packed beds into the computational domain. Cooper and Hallet [12] modelled a one-dimensional char bed in which char particles advance downwards through the bed. Thunman and Leckner [13] proposed a similar one-dimensional model with some advances in the calculation of bed shrinkage during thermal conversion. Yang et al. [14] used a mesh for the packed bed to solve several variables representing the solid phase state of combustion, but this mesh was out of the flow computational domain. Collazo et al. [15] and Gómez et al. [16] proposed three-dimensional models that implement the bed with the gas flow through the use of user defined variables to account for the combustion stages and heat and mass exchanges. A higher level of complexity is the thermally thick consideration, which is the modelling of thermal (and compositional) gradients inside the biomass particles. Yang et al. [17] created a two-dimensional model in which particles were discretised and internal gradients were calculated. Thunman et al. [18] proposed a particle model that used an internal subgrid scale to model the particle layers and the advance of these layers towards the centre of the particle. This approach was used by Mehrabian et al. [19,20] and Ström and Thunman [21] for three-dimensional packed beds. Gómez et al. [22] used a similar subgrid scale with an efficient solution algorithm based on the numerical heat transfer techniques to calculate all the volumes and temperatures of the particle layers in one step and tested the model at the particle and bed scales. The same approach was adapted to a domestic boiler [23]. Other researchers focused their models on the particle and solved the bed as the contribution of each individual particle. Peters and Bruch [24] used a discrete phase model (DPM) to calculate the particle dynamics and conversion and calculated a one-dimensional bed. Wiese et al. [25] separately calculated the particle dynamics using a discrete element model (DEM) and introduced the results in a CFD computational domain to calculate the gas phase dynamics.

One of the main advantages of the use of this model is the possibility to study a boiler's performance in a large variety of operating conditions, especially when the costs of experimental facilities are high. A field with a growing interest is the study of firing conditions with different gas blends. An example of this is the oxy-fuel firing, which has been investigated in the latest years by several studies to reduce the costs of CO_2 separation and to improve the efficiency of coal industrial boilers with reduced contaminant emissions. Several works used numerical modelling to study the oxy-fuel combustion [26,27]. Another field of study is the combustion with enriched air, which is used to increase the efficiency in high temperature processes. However, only a limited number of studies were performed in biomass combustion with enriched air [28,29].

This paper presents a model that uses CFD techniques to calculate the working of a biomass boiler in a fast and stable simulation with reasonably high accuracy and without great computational effort. The biomass packed bed is represented as a porous region and the temperature of the bed is calculated as a user defined variable. The thermal conversion of biomass is modelled through reactive fluxes that introduce in the packed bed the source terms of mass, energy, and species representing the products of the combustion stages. The heat and mass transfer are calculated through several submodels that were tested in previous works. The overall behaviour of the model is tested by simulating experimental tests in a small-scale boiler with reasonably good results with respect to the heat transferred and gas

emissions. This same boiler is simulated to analyse the effect of oxygen enrichment in the energy performance and contaminant emissions.

2. Model Description

Since the CFD codes are not prepared to simulate the solid biomass combustion phenomena, a combination of models is proposed in this work. The overall modelling predicts the behaviour of the boiler operating in steady conditions which means a fast-solution procedure with low computational costs. The packed bed is modelled as a porous region, and the products of biomass combustion are introduced as source terms of the mass energy and species in this region. Therefore, the mass introduced in the domain is not the solid fuel but the products of the thermal conversion of that solid fuel (volatile matter and the corresponding energy). These fluxes are introduced as volumetric sources. All the calculations are performed through user defined functions (UDFs) that are included in the CFD code. The main limitation of this model is the fact that the shape of the bed is fixed; it is estimated approximately, but it is not calculated by the model. That would need a high number variables and surely transient calculations until the final bed shape is reached for each case. Therefore, this model is applicable for cases in which approximate bed geometry is known. The solid fraction is a constant value in the whole bed with a value of 0.56 which was measured the raw fuel.

2.1. Assumptions

To simplify the complex phenomena of thermal conversion in a fast-solution method, several assumptions are necessary.

- The porous medium is modelled as a disperse medium with local volume-averaged properties within each computational cell.
- An average conversion state is considered to represent a steady combustion point.
- The packed bed size and shape must be known initially.
- The whole biomass content is consumed.
- The devolatilisation rate is homogeneous in the whole packed bed.
- Char reactions are distributed according to the presence of reactants.
- The gas–solid heat exchange is performed by convection and radiation. The solids also exchange heat by conduction and radiation.
- An ideal gas is assumed in the mixture.

2.2. Solid Phase

As said above, the solid phase is modelled as a disperse porous medium in which products of combustion are introduced. In each cell of the bed, the drying, devolatilisation and char combustion fluxes are distributed inside the bed depending on the bed temperature. It is not necessary any particle subgrid since it is a steady model. This fact reduces notably the computational effort. The gases and energy introduced in the bed react in the boiler freeboard, and the energy exchanged by the packed bed and freeboard keeps the combustion active. This process is represented in Figure 1. To model this interaction, a solid enthalpy variable is created to represent the solid phase temperature in the bed region. This variable follows the steady transport Equation (1). The fluxes of the species that represent the gas phase mixture are introduced proportionally to the consumption rates of the biomass species. The rate of H_2O from drying (Equation (2)), the volatile k species from devolatilisation (3), and the k products of the heterogeneous char reactions (4) are calculated by considering the mass flow rate of biomass and the fractions given by the proximate analysis. The difference between the heat value

of the solid fuel and the reaction enthalpy of the generated species is introduced in the solid energy equation as a source term to balance the energy conservation (Equation (5)).

$$\frac{\partial(\varepsilon\rho_p h_s)}{\partial t} = \nabla(k_s \cdot \nabla T_s) + S_{h_s} \tag{1}$$

$$\dot{\omega}'''_{H_2O,m} = \dot{\omega}'''_f Y_m \tag{2}$$

$$\varphi\dot{\omega}'''_{k,v} = \dot{\omega}'''_f Y_v \gamma_k \tag{3}$$

$$\dot{\omega}'''_{k,c} = \dot{\omega}'''_f Y_c \cdot \Gamma_k \tag{4}$$

$$S_{h_s} = \dot{\omega}'''_f \left(LHV - \sum_j Y_j h_j^R \right) \tag{5}$$

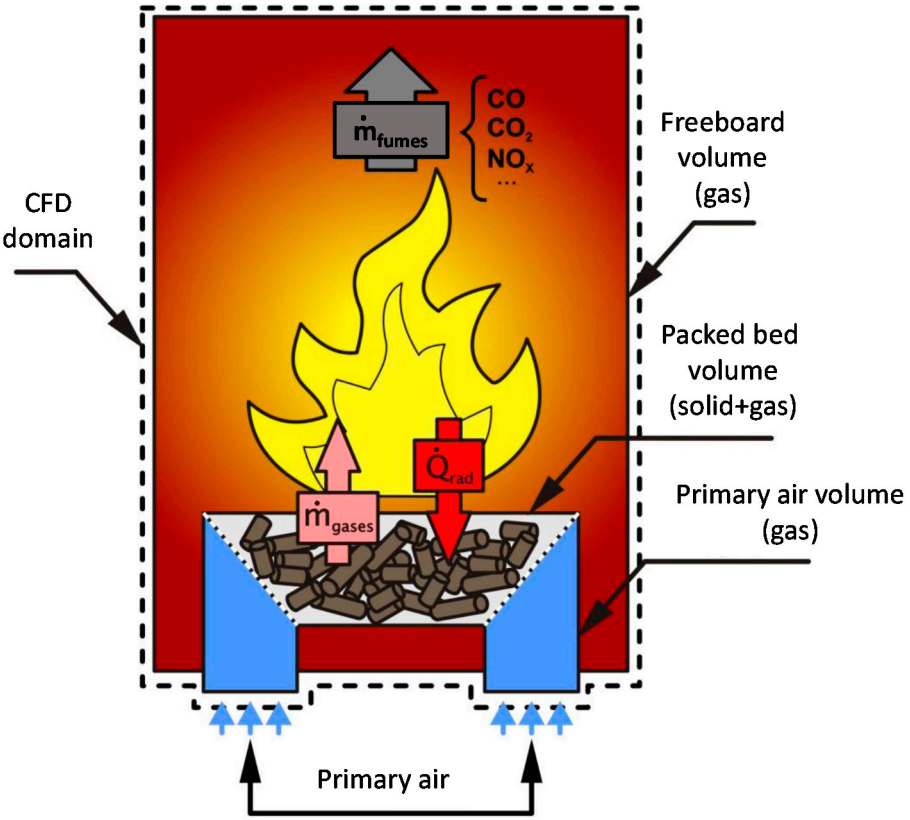

Figure 1. Representation of the combustion approach.

The devolatilisation is modelled as the rate of conversion of the volatile content, and it is considered to occur at the solid phase temperature calculated following Equation (1). The char combustion is modelled as the direct char oxidation, (R.1) [30], and two gasification reactions, (R.2) and (R.3) [31], and the kinetics in these reactions (K_g^{ox}, $K_g^{g,1}$ and $K_g^{g,2}$, respectively) are shown in Table 1. The char oxidation CO/CO_2 ratio is governed by the parameter φ, as shown in (6). The char reactions are controlled thermally and by the reactants' diffusion. The global coefficients of these reactions are shown in the Equation (7).

$$\varphi = \frac{2 + 4.3\exp\left(\frac{-3390}{T_s}\right)}{2\left(1 + 4.3\exp\left(\frac{-3390}{T_s}\right)\right)} \tag{6}$$

$$K_{glob}^{ox} = \frac{1}{\frac{1}{K^{ox}} + \frac{1}{K_m^{ox}}},\ K_{glob}^{g,1} = \frac{1}{\frac{1}{K^{g,1}} + \frac{1}{K_m^{g,1}}},\ K_{glob}^{g,2} = \frac{1}{\frac{1}{K^{g,2}} + \frac{1}{K_m^{g,2}}} \quad (7)$$

Table 1. Kinetics of the solid heterogeneous reactions.

	Heterogeneous Char Reactions	Kinetics
(R.1)	$C + \varphi O_2 \rightarrow 2(1-\varphi)CO + (2\varphi - 1)CO_2$	$K^{ox} = 1.715 \cdot T_s \cdot exp\left(-\frac{9000}{T_s}\right)$
(R.2)	$C + CO_2 \rightarrow 2CO$	$K^{g,1} = 3.42 \cdot T_s \cdot exp\left(-\frac{1.56\times10^4}{T_s}\right)$
(R.3)	$C + H_2O \rightarrow CO + H_2$	$K^{g,2} = 5.7114 \cdot T_s \cdot exp\left(-\frac{1.56\times10^4}{T_s}\right)$

2.3. Gas Phase

The gas phase is modelled though the conservation of the continuity, momentum, energy, turbulence, and chemical species. Commercial CFD software is widely developed to solve these equations through finite volumes methods. In this work, the spatial discretisation is solved with the second-order upwind method for all equations except the turbulence since the first order scheme gives a better convergence. The pressure is solved with PRESTO. The radiation transport is solved with a modification of the discrete ordinate model (DOM) explained below. The realisable k-ε model is used to model the turbulence.

The conversion of biomass into gaseous products is performed by generating gas species in the bed with the biomass combustion rates (Equations (2)–(4)). These species are water vapour from drying, the volatile species during devolatilisation, and the CO, CO_2, and H_2O from the heterogeneous char reactions. The volatiles emitted during devolatilisation are composed mainly of tars (represented by C_6H_6), light hydrocarbons (represented by CH_4), CO, CO_2, H_2, and H_2O [32]. The composition of the volatiles emitted during devolatilisation is estimated through the balance proposed by Thunman et al. [33].

The interaction between the packed bed and the flow is introduced as a source in the momentum equation (Equation (8)). This term depends on the permeability and inertial resistance coefficients shown in Equations (9) and (10), respectively.

$$S_{mom} = -\left(\frac{\mu}{\eta} v_\infty + \Upsilon \frac{1}{2} \rho_g v_\infty^2\right) \quad (8)$$

$$\eta = \frac{\psi^2 d_{eq}^2}{150} \frac{(1-\varepsilon)^3}{\varepsilon^2} \quad (9)$$

$$\Upsilon = \frac{3.5}{\psi\, d_{eq}} \frac{\varepsilon}{(1-\varepsilon)^3} \quad (10)$$

A set of seven chemical reactions is introduced to model the gas phase reaction scheme used by the authors in previous papers [16,34,35]. This scheme is composed by the partial oxidation of hydrocarbons from wood devolatilisation (benzene (R.4) and methane (R.5)) and hydrogen (R.6)) [15,16] to carbon monoxide. The complete combustion of hydrocarbons is reached through the oxidation of CO to CO_2 (R.7) and a two-way reaction of water and carbon monoxide ((R.8) and (R.9)) [36,37]. The reaction scheme is completed by the NH_3 conversion to NO and N_2 and the two-step mechanism of Brink [38] was used. The monoxide reactions ((R.10) and (R.11)) show the two steps of the oxidation of ammonia using NO as an intermediate species.

$$C_6H_6 + \frac{9}{2} O_2 \rightarrow 6\,CO + 3\,H_2O \quad (R.4)$$

$$CH_4 + \frac{3}{2}\,O_2 \rightarrow CO + 2\,H_2O \quad (R.5)$$

$$H_2 + \frac{1}{2}O_2 \rightarrow H_2O \quad \text{(R.6)}$$

$$CO + \frac{1}{2}O_2 \rightarrow CO_2 \quad \text{(R.7)}$$

$$H_2O + CO \rightarrow CO_2 + H_2 \quad \text{(R.8)}$$

$$CO_2 + H_2 \rightarrow H_2O + CO \quad \text{(R.9)}$$

$$NH_3 + O_2 \rightarrow NO + H_2O + \frac{1}{2}H_2 \quad \text{(R.10)}$$

$$NH_3 + NO \rightarrow N_2 + H_2O + \frac{1}{2}H_2 \quad \text{(R.11)}$$

2.4. Heat and Mass Transfer

The heat and mass transfer processes play a key role in solid biomass combustion. The modelling of these phenomena is modelled in the CFD code through the diffusion coefficients and the source terms in the equations of mass energy and species. The heat diffusion through the packed bed is modelled by a thermal conductivity coefficient, which was experimentally obtained. This coefficient is 0.17 ($W{\cdot}m^{-1}{\cdot}K^{-1}$) for a bed of wood particles and 0.12 ($W{\cdot}m^{-1}{\cdot}K^{-1}$) for a bed of char particles. The global conductivity is obtained by a mass weighted average.

The heat transferred between biomass particles and gas flow is modelled as a source term in both energy equations of the solid and gas phases. This source term follows Equation (11). The convective coefficient is calculated as shown in Equation (12), and the Nusselt number is estimated by the correlation proposed by Wakao et al. [39] (Equation (13)). An analogous formulation is used for calculating the mass transfer coefficients K_m^{ox}, $K_m^{g,1}$ and $K_m^{g,2}$ that affect the heterogeneous char reactions. These coefficients follow Equation (14), and the Sherwood dimensionless number is calculated analogous to the Nusselt number (Equation (15)).

$$S_s^{conv} = -S_g^{conv} = hA_v\left(T_g - T_s\right) \quad (11)$$

$$h = \frac{Nu{\cdot}k_g}{d_{eq}} \quad (12)$$

$$Nu = 2 + 1.1{\cdot}\ Re^{0.6}{\cdot}Pr^{\frac{1}{3}} \quad (13)$$

$$k_m^i = \frac{Sh{\cdot}Di_i}{d_{eq}} \quad (14)$$

$$Sh = 2 + 1.1{\cdot}\ Re^{0.6}{\cdot}Sc^{\frac{1}{3}} \quad (15)$$

2.5. Modelling Radiation

Radiation is the most relevant way of heat transfer in high temperature systems. In biomass combustion, radiation plays an important role in the heat exchange between the packed bed and the flame as well as between biomass particles inside the bed. In this work, the method presented by the authors in a previous work [40] is used to model the radiation in porous media. A modification of the discrete ordinates model (DOM) is used to take into account the participation of both solid and gas phases in the packed bed.

Several parameters and source terms are introduced in the transport equations of solid phase energy, gas phase energy, and radiation intensity to change the default radiative transfer equation (RTE) to a modified RTE that considers both solid and gas phases for the absorption, emission, and scattering terms (Equation (16)). In addition, the corresponding source terms are introduced in the energy equation of solid and gas phases, as shown in Equations (17) and (18), respectively. A schematic of the

modified D.O. model is shown in Figure 2. The details of the changes needed to introduce the CFD code Ansys Fluent to work with this model are explained in [40].

(16)

$$S_s^{rad} = \int_0^{4\pi} \left(\alpha_s I(\boldsymbol{r}, \boldsymbol{s}) - \frac{\alpha_s n^2 \sigma {T_s}^4}{\pi} \right) d\Omega \quad (17)$$

$$S_g^{rad} = \int_0^{4\pi} \left(\alpha_g I(\boldsymbol{r}, \boldsymbol{s}) - \frac{\alpha_g n^2 \sigma {T_g}^4}{\pi} \right) d\Omega \quad (18)$$

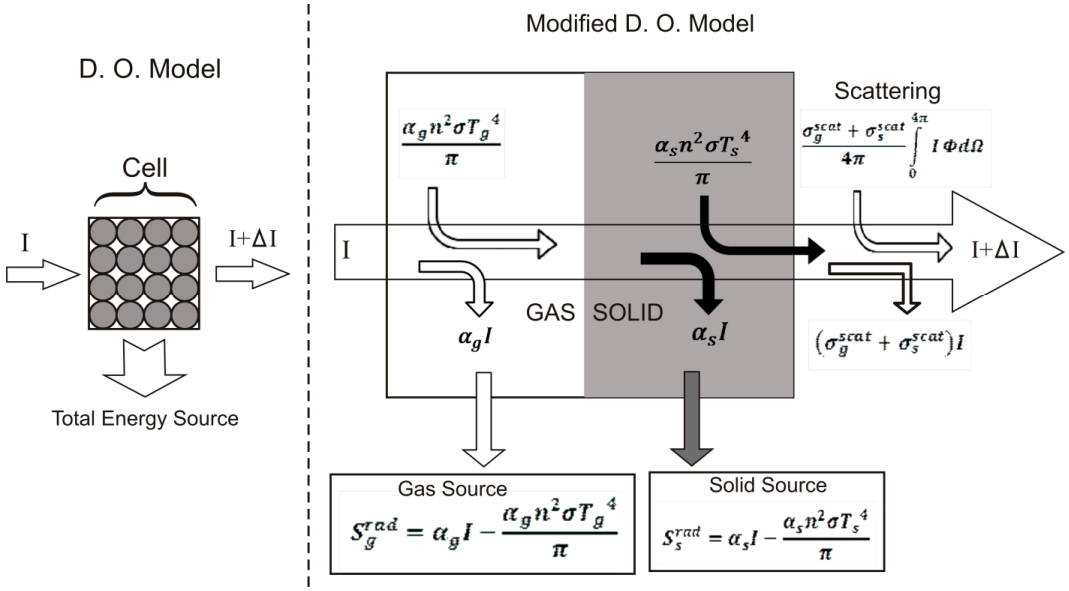

Figure 2. Scheme of the modification of the D.O. radiation model for a direction [40].

The approach of this method is treating the porous region as a semitransparent media using the absorption and scattering coefficients to characterize the bed. An extinction coefficient for a bed of particles can be calculated through the formulation proposed by Shin and Choi [41] (Equation (19)) as a function of the particle diameter and the porosity of the medium. The absorption and scattering coefficients can be related to the extinction coefficient through the surface absorptivity of the particles (Equations (20) and (21), respectively) under the hypothesis of diffuse reflectivity.

$$\beta_s = -\frac{1}{d_{eq}} ln(1 - \varepsilon) \quad (19)$$

$$\alpha_s = Ab \cdot \beta_s \quad (20)$$

$$\beta_s = \alpha_s + \sigma_s^{scat} \quad (21)$$

3. Simulated Plant and Fuel

3.1. Experimental Boiler

The proposed model was applied in a commercial pellet boiler (KWB Multifire) represented in Figure 3. This boiler operates by introducing the fuel from the bottom of a grate in which a primary air injection is introduced from several holes arranged in a circular pattern. Over the grate, in the boiler furnace, a ring-shaped injector feeds the flame through a secondary air flux. This secondary injection is orientated to generate swirl and improve the turbulence and gas mixing. The furnace walls are cooled, with the exception of the frontal wall, where a door is placed. Over the furnace, a dome is located to prevent the flame from reaching the cooled tubes of the heat exchanger, which would

produce a flame quenching with negative consequences in the boiler performance and contaminant emissions. Fifteen tubes composed the heat exchanger and several spiral praises are located in the tubes to increase the heat transferred to the cooled walls.

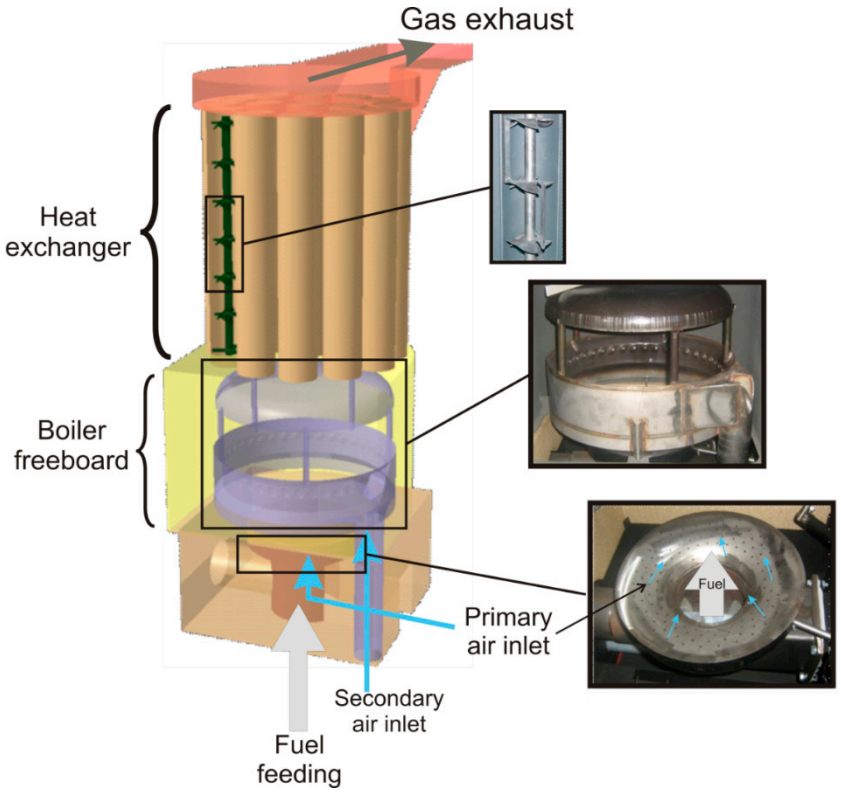

Figure 3. Scheme of the commercial boiler used in the experiments.

3.2. Fuel Properties

The fuel used for this work was pinewood biomass whose particles are compacted pellets. The data of the proximate analysis and the main particle properties are shown in Table 2.

Table 2. Composition and properties of the fuel.

Proximate Analysis		Fuel Properties	
Moisture (wt %, a.r.)	6.8	Equivalent formulation (dbaf)	$CH_{1.57}O_{0.74}N_{0.0025}$
Ash (wt %, a.r.)	0.3	Density (ρ) (kg·m^{-3})	1200
Fixed Carbon (wt %, a.r.)	24.4	Equivalent diameter ($_{deq}$) (mm)	8.8
Volatile matter (wt %, a.r.)	68.5	Sphericity	0.85
LHV (MJ/kg, a.r.)	16.17	Solid fraction (ε)	0.56

3.3. Mesh Details and Boundary Conditions

Several meshes of the boiler geometry were used to test the model and ensure its behaviour with special care on overall behaviour of the boiler in parameter such as heat transferred, contaminant emissions, and the reactive areas inside the freeboard. No significant changes were observed for grids with elements smaller than 10 mm side. A final polyhedral mesh of approximately 1.5 million elements was used to model the boiler geometry which is enough to obtain a reasonably good resolution. The average length of the cells was approximately 6 mm. In addition, the most critical regions for combustion and heat transfer were meshed with a special refinement. These zones are the bed region, especially near the air injections, the flame zone and the cooled tubes of the heat exchanger. Average cell sizes of 3 mm and 5 mm were used in the bed and heat exchanger regions respectively.

Figure 4 shows the details of the main boundary conditions with the boundary surfaces marked. The walls conditions are common for all the simulated cases. Otherwise, the mass fluxes introduced at the inlets and the ratio of oxygen and nitrogen are different for every simulated case, either for the experimental contrast and the oxygen concentration study sections. Five-percent of turbulence intensity and the hydraulic diameter of the inlets are introduced as turbulence parameters and the turbulence level is calculated through the realisable k-ε model across the air course, the air injections and the flame region, where turbulence is a key parameter in the combustion development. In this case, both primary and secondary air inlets are located quite far from the correspondent injections. Therefore, the inlet parameters hardly influence to the air injections.

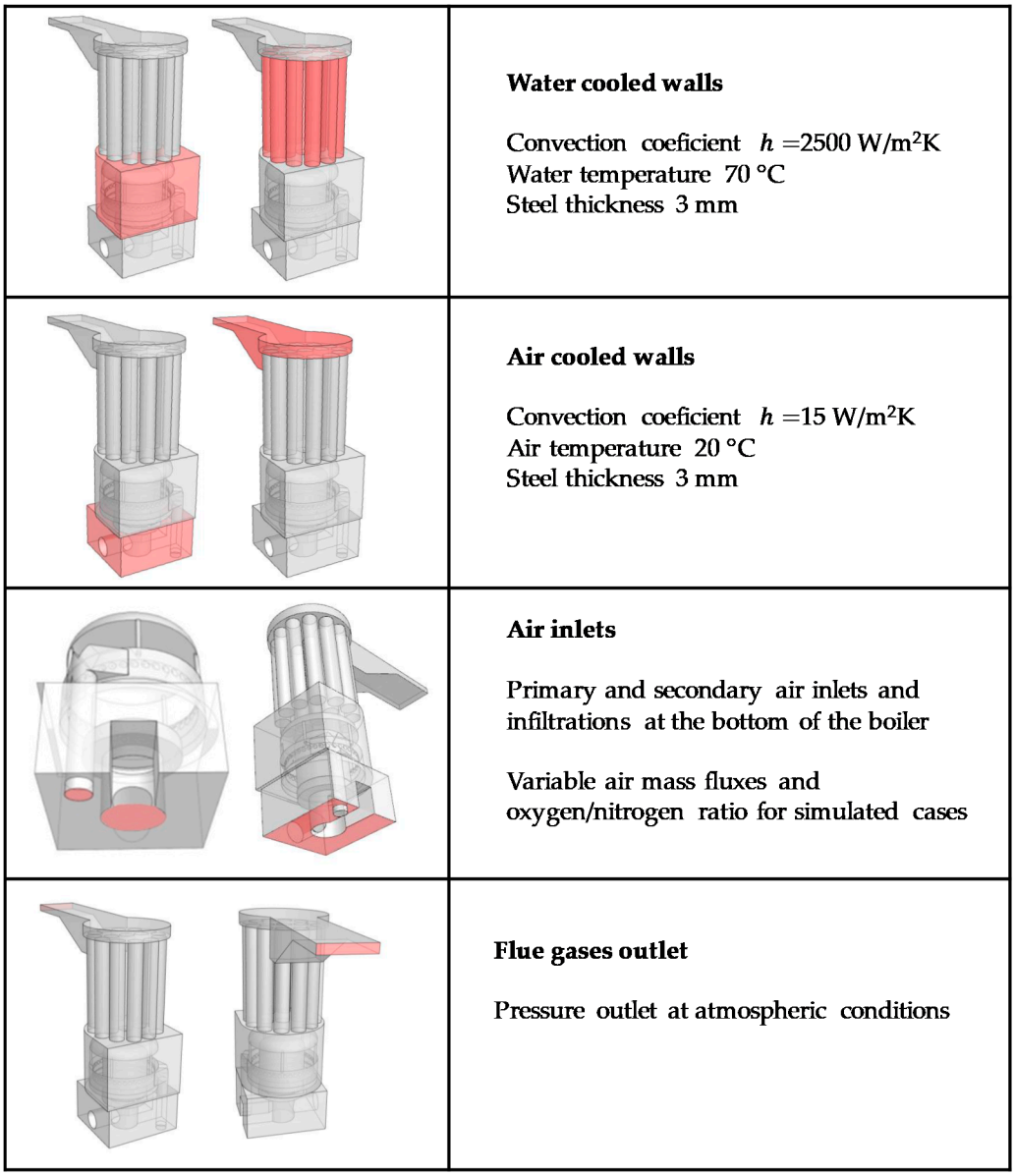

Figure 4. Main boundary conditions of the boiler model.

4. Results and Discussion

4.1. Experimental Contrast

An experimental plant was built to measure the main operating parameters of the boiler. The scheme of this plant is shown in Figure 5. The setup is composed of three flow meters located in

the primary and secondary air inlets and in the exhaust tube to measure both the air injections and air infiltrations. A gas analyser is also located in the exhaust tube to report the flue gases temperature and volumetric concentrations of contaminants. The water circuit is also equipped with a flow meter and thermocouples to calculate the heat transferred to the water.

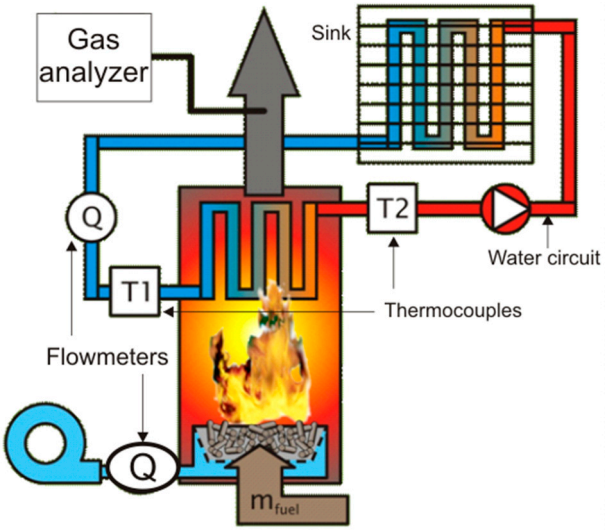

Figure 5. Schematic of the experimental setup.

The proposed model was tested in two experiments (E1 and E2) performed in the boiler by changing the rates of the primary and secondary air fluxes. In both cases, the boiler operates with a fuel mass flux equivalent to 36.5 kW. The flow meter measurements give the primary and secondary air fluxes as well as the flux of the unavoidable infiltrations. All these fluxes are shown in Table 3. The water temperature of the boiler was 70 °C for all of the tests.

Table 3. Operating conditions for the experimental tests.

Test	Fuel Feeding Rate ($g \cdot s^{-1}$)	Primary Air Flow Rate ($g \cdot s^{-1}$)	Secondary Air Flow Rate ($g \cdot s^{-1}$)	Air Infiltration ($g \cdot s^{-1}$)
E1	2.26	4.7 (13%)	9.6 (27%)	20.6 (60%)
E2	2.26	7.3 (22%)	8.0 (24%)	17.6 (54%)

The comparison between the model's predictions and experimental data collected from both tests is shown in Figure 6. Parameters such as the heat exchanged, fumes temperature and emissions of CO_2, CO, and NO_x are compared.

Despite the fact that these parameters are measured far from the flame region and, consequently, that the model cannot be validated for the flame prediction, it can be useful to predict the general behaviour of the boiler for the study of the performance and gas emissions.

The simulations of both tests E1 and E2 show close results between the predictions and experimental data in parameters such as the heat transferred to water and the fumes temperature, as shown in Figure 6. Maximum discrepancies of 5% and 3.5% were found in the power and fumes temperatures, respectively. The deviations in the predictions of the CO_2 concentrations in fumes are reasonably low. These discrepancies can be caused by the uncertainties in the composition of fuel and small errors in the mass conservation in the prediction of volatiles' composition since the carbon balance is ensured in the whole simulation process. The predictions of the CO and NO_x emissions give results reasonably close to the experiments considering the simplicity of the CO and NO reaction mechanisms.

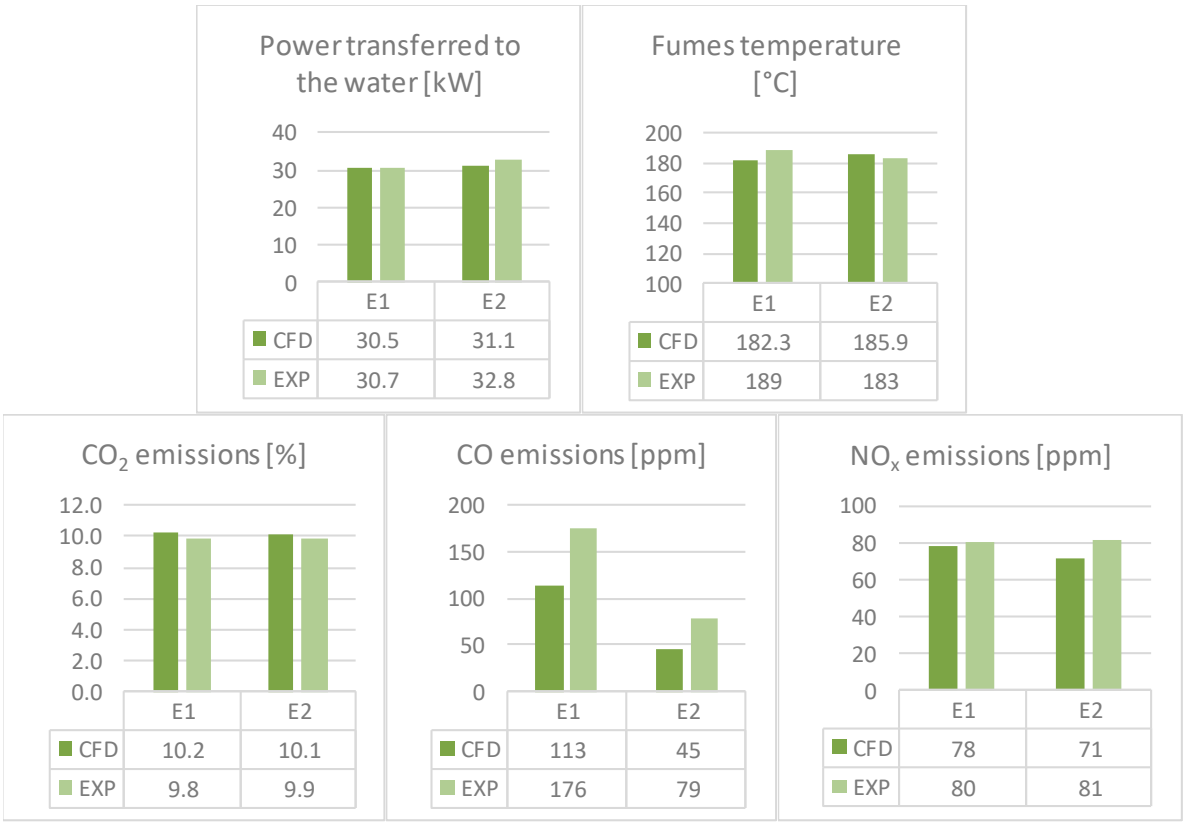

Figure 6. Experimental results vs. model prediction.

4.2. Numerical Study of the Effect of Oxygen Concentration

This study is focused on analysing the behaviour of the boiler when it is fed with different oxygen concentrations. The boiler was simulated by using the models described above, and the most critical parameters in the performance and contaminant emissions are analysed in this section. The oxygen concentration varied from the concentration in air (21% volumetric) to 90%, and the air flux was reduced to keep the oxygen mass flow of the experiment E1 shown in Section 4.1. The ratios of the primary air, secondary air, and infiltration were also kept using experiment E1 as a reference.

Figure 7 shows the scalar fields of the gas temperature and oxygen mole fraction in the middle plane of the boiler. The reaction zone in the centre of the furnace causes an increase in temperature, which is decreased in the surroundings of the furnace and in the tubes of the heat exchanger due to the contact with the cooled walls. The reaction zone is more concentrated when the oxygen concentration is increased, and the maximum temperature is also higher due to the lower mass flow rate of gases. The maximum temperatures found in the furnace were 1750 K with 21% O_2 in the inlets and 2050 K with 90% O_2. The temperature decrease in the heat exchanger is more pronounced when increasing the O_2 since the total mass flow rate of gases is lower. In this way, the gas flux is more sensitive to the cooling process and the heat exchange is more effective. The oxygen mole fraction in the furnace is, as expected, increased when a high concentration is introduced in the inlets, which stimulates the secondary gas reactions to complete the combustion of the intermediate species. Therefore, lower CO emissions are expected. The gas temperature has an important influence to activate the pyrolysis of the bed. As the extinction coefficient in the bed zone is high (Equation (19)), most of incident radiation is extinguish in only a few millimetres deep. Therefore, most radiation is absorbed by the first two layers of particles.

Figure 8 shows the CO molar fraction in the boiler furnace for the same O_2 concentrations in the inlets as Figure 7. It shows a more concentrated reaction zone when O_2 is increased and a smaller flame than the original case (21% O_2). This scenario helps the CO consumption since the higher CO

concentration coincides with the higher flame temperatures. Figure 9 shows the temperature field of the solid phase in the packed bed. All cases show a similar temperature distribution. A higher temperature region is located over the air injection on the grate. This is caused mainly by the char oxidation reaction, which releases a high amount of energy. Temperatures of approximately 1400 K are reached at this region. The air enrichment favours the char oxidation as well as the volatiles reactions, which causes an overall higher temperature in the bed. As a high extinction coefficient is found in the packed bed (approximately 120 (m^{-1})), the high temperatures reached produce an important emission of radiation. This has an important influence in heat transfer and the distribution of temperatures in the freeboard.

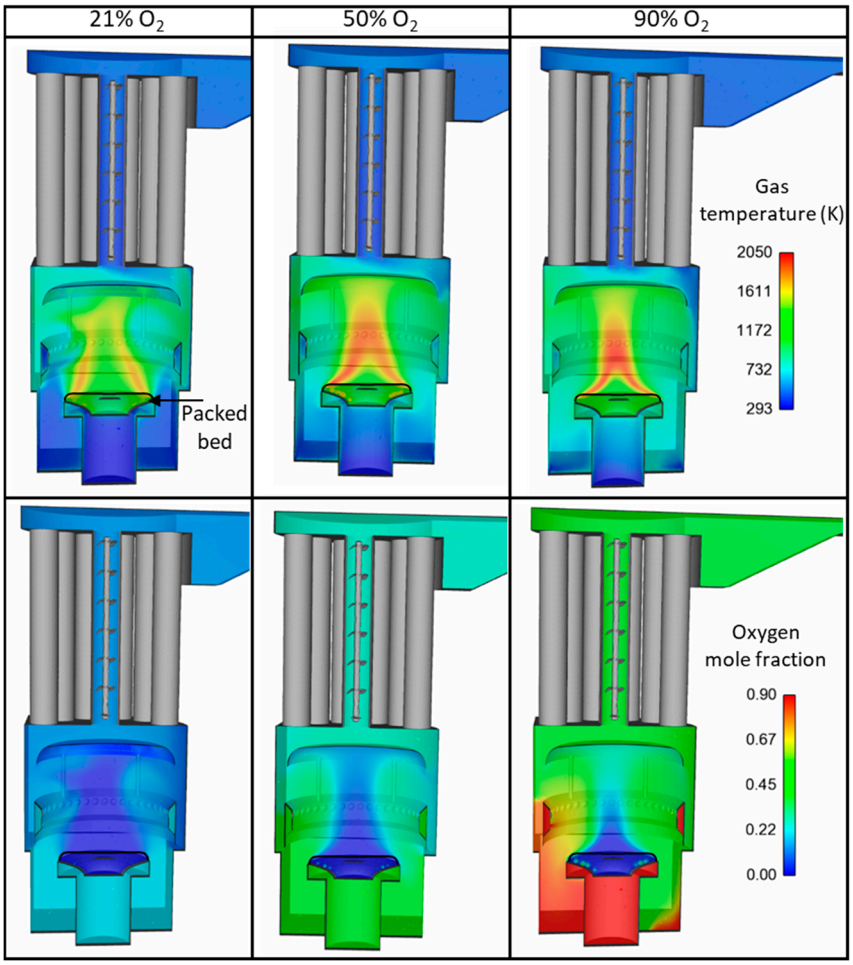

Figure 7. Contours of the gas temperature and oxygen concentration inside the boiler for the simulations of 21%, 50%, and 90% of oxygen in the inlets.

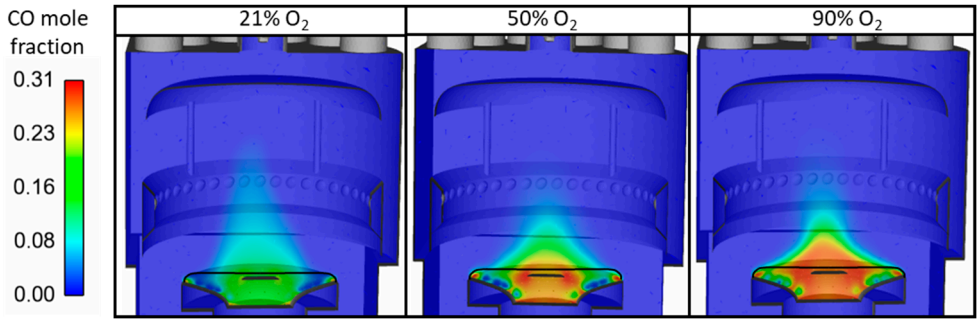

Figure 8. Contours of the CO mole fraction inside the boiler for the simulations of 21%, 50%, and 90% of oxygen in the inlets.

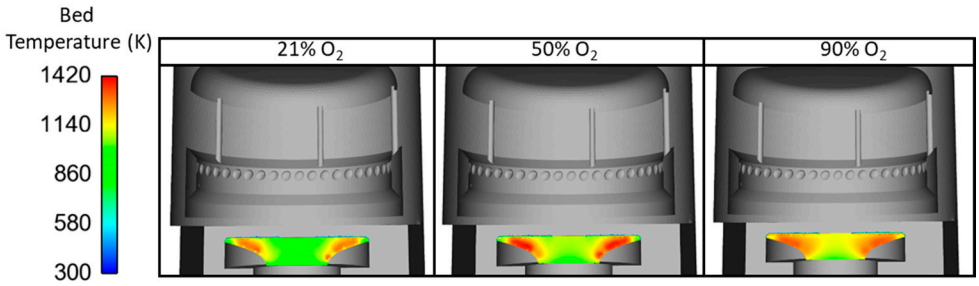

Figure 9. Contours of the packed bed temperature for the simulations of 21%, 50%, and 90% of oxygen in the inlets.

The effect of oxygen enrichment in the boiler performance can be studied through the analysis of the power transferred to the water circuit and the fumes temperature. Figure 10 shows the influence of the oxygen enrichment in both parameters. As expected, the power transferred to the water is increased with a higher oxygen concentration, which improves the boiler's thermal performance. The most interesting aspect is that main improvement takes place when the oxygen concentration is increased up to 40%. This result means that an important improvement can be reached with moderate air enrichment. The figure also shows that the fumes temperature decreases with the oxygen enrichment. Despite the lower gas flux in the boiler, which increases the combustion gases inside the boiler, the heat transfer to the cooled walls is more effective since the thermal inertia of the flow is much lower. This effect is caused due to the lack of nitrogen in the gas stream. The increase of oxygen concentration is due to a nitrogen reduction since the boiler operates with the same oxygen excess index. In addition, the specific heat of oxygen is lower than that of nitrogen.

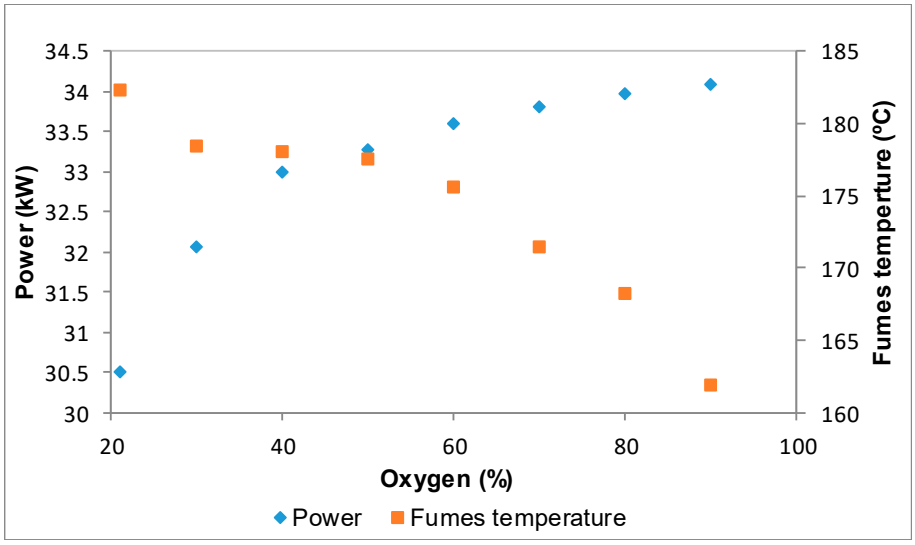

Figure 10. Effect of the oxygen enrichment in the power transferred to water and fumes temperature.

Figure 11 shows the effect of the oxygen enrichment in the emissions of CO and CO_2. As expected, the CO_2 concentration in fumes is increased with the oxygen concentration since the total flow of fumes is lower due to the lack of nitrogen. Nevertheless, the CO concentration in fumes is strongly decreased when the oxygen concentration increases to 30%. With higher oxygen concentrations, only small improvements are reached. This result means a more efficient combustion is reached with moderate oxygen enrichment. This improvement in the combustion of CO is caused by the oxygen availability and the higher temperatures that are reached in the flame region. Figure 12 shows the NO_x emissions in the whole range of oxygen concentrations. It shows that the NO_x molar fraction in fumes is increased with the oxygen enrichment. This effect is expected due to the lack of nitrogen, and thus, the total

NO_x mass flux is also shown to visualise the actual effects in emissions. Although an abrupt increase in emissions occurs with 30% O_2, the emissions decrease to closer values than the original emissions for 40% and 50% O_2, and the NO_x mass flux is increased again for high O_2 concentrations. Most of the NO_x present in the flue gases comes from the nitrogen content of the fuel. NO_x emissions from the fuel were calculated for all cases and, then, thermal NO_x emissions were calculated as a Fluent postprocessing calculation. The thermal NO_x that is detected is negligible in comparison.

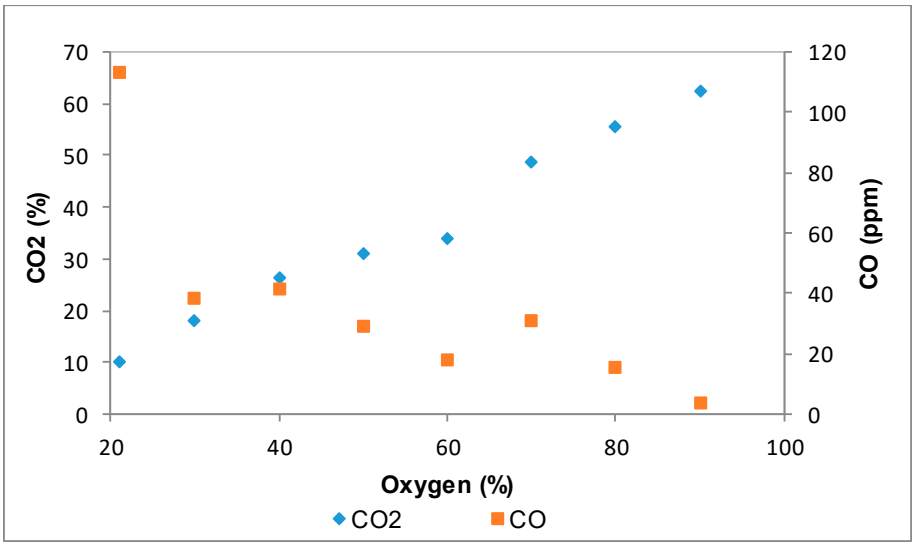

Figure 11. Effect of the oxygen enrichment on the emissions of CO_2 and CO.

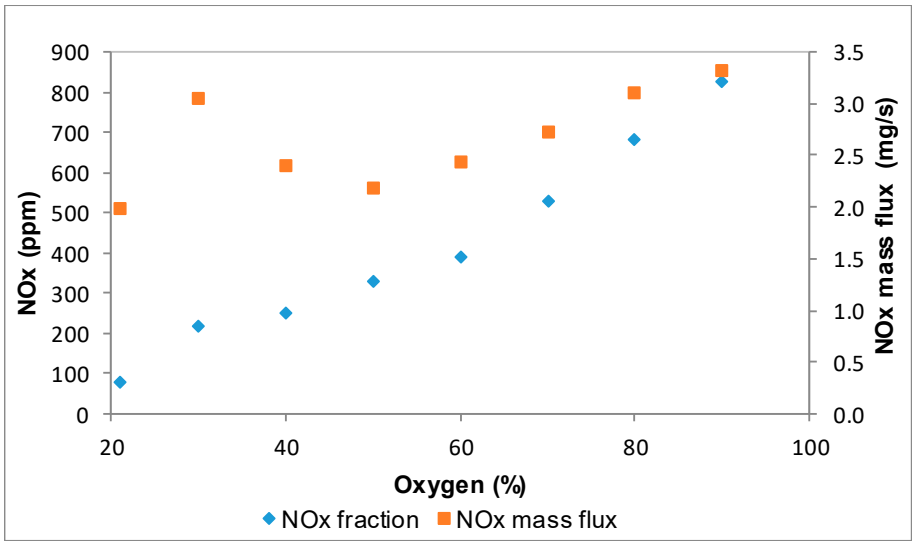

Figure 12. NO_x emissions for different conditions of oxygen enrichment.

5. Conclusions

This paper presents a model to simulate the overall behaviour of a small-scale biomass boiler, and the model is applied to study the effect of the oxygen enrichment supplied air. The model contributes to an efficient calculation with low computational costs that can be useful to the analysis and design of boilers and combustion systems. The thermal conversion of solid biomass is modelled through heat transfer and mass fluxes in the packed bed region, and the combustion is completed in the gas phase through the transport and reaction phenomena. The model is applied to the simulation of two experimental tests and parameters such as the transferred heat, temperature of fumes, and gas emissions are compared with the experiments with reasonably good predictions. The study of the

oxygen enrichment in the feeding air shows improvements of the transferred heat and a reduction of the fumes temperature when the air is enriched. The energy efficiency can be increased to approximately a 12% by increasing the oxygen concentration. Nevertheless, an improvement of 8% can be reached for an oxygen concentration of 40%. The emissions of CO decrease abruptly for a moderate oxygen enrichment, and the NO_x emissions increase noticeably for a 30% of oxygen concentration but then decrease for 40%. The global analysis shows that an air enrichment of 40–50% of oxygen leads to noticeable improvements in the boiler performance and CO emissions by keeping the NO_x of the air firing conditions.

Author Contributions: M.A.G. developed the models, performed the numerical simulations and collaborated in the manuscript write up. R.M. collaborated in the manuscript write up and results post processing. J.C. collaborated in the experimental tests and supervised the article writing. J.P. collaborated in the experimental tests and article supervision and led the project planning.

Funding: This research received financial support from the Project ENE2015-67439-R of the Ministry of Economy of Spain.

Conflicts of Interest: The authors declare no conflicts of interest.

Nomenclature

Ab	Absorptivity
A_v	Area-volume ratio (m^{-1})
d_{eq}	Equivalent diameter (m)
Di_i	Diffusivity of the species i in the mixture ($m^2 \cdot s^{-1}$)
h	Convection coefficient ($W \cdot m^{-2} \cdot K^{-1}$)
h_s	Solid phase enthalpy ($J \cdot kg^{-1}$)
h_f^0	Reaction enthalpy ($J\ kg^{-1}$)
I	Irradiation intensity ($W \cdot m^{-2} \cdot sr$)
k	Thermal conductivity ($W \cdot m^{-1} \cdot K^{-1}$)
K	Char reaction constants ($m \cdot s^{-1}$)
km	Mass transfer constant ($m \cdot s^{-1}$)
LHV	Lower heat value ($J \cdot kg^{-1}$)
Nu	Nusselt number (-)
n	Refractive index (-)
Re	Reynolds number (-)
r	Position vector (m)
s	Direction vector (m)
$s´$	Scattering direction vector (-)
Pr	Prandtl number (-)
Sh	Sherwood number (-)
Sc	Schmidt number (-)
S	Source term ($W \cdot m^{-3}$)
T	Temperature (K)
t	Time (s)
v_∞	Gas velocity ($m \cdot s^{-1}$)
Y	Mass fraction
Greek	
α	Absorption coefficient (m^{-1})
β	Extinction coefficient (m^{-1})
γ	Mass fraction of species generated in the bed (-)
ε	Solid fraction (-)
μ	Viscosity ($kg \cdot m^{-1}\ s^{-1}$)
σ	Stefan–Boltzmann coefficient ($W \cdot m^{-2}\ K^{-4}$)
σ^{scat}	Scattering coefficient (m^{-1})
Γ	Stoichiometric coefficient

Y	Inertial resistance factor (m^{-1})
η	Permeability [m^2]
ρ	Density ($kg \cdot m^{-3}$)
φ	Char oxidation parameter (-)
Φ	Scattering function (-)
ψ	Sphericity (-)
$\dot{\omega}_i$	Generation or consumption rates of the wood components ($kg \cdot m^{-3} \cdot s^{-1}$)
Ω	Solid angle (sr)

Subscripts

c	Char
f	Fuel
g	Gas
glob	Global
m	Moisture
p	Particle
s	Solid
v	Volatile species

Superscripts

conv	Convection
g,1	Gasification reaction with CO_2
g,2	Gasification reaction with H_2O
ox	Char oxidation
rad	Radiation

References

1. Abagnale, C.; Cameretti, M.C.; De Robbio, R.; Tuccillo, R. Thermal cycle and combustion analysis of a solar-assisted micro gas turbine. *Energies* **2017**, *10*, 773. [CrossRef]
2. Kim, G.; Moon, S.; Lee, S.; Min, K. Numerical analysis of the combustion and emission characteristics of diesel engines with multiple injection strategies using a modified 2-D flamelet model. *Energies* **2017**, *10*, 1292. [CrossRef]
3. Chaney, J.; Liu, H.; Li, J. An overview of CFD modelling of small-scale fixed-bed biomass pellet boilers with preliminary results from a simplified approach. *Energy Convers. Manag.* **2012**, *63*, 149–156. [CrossRef]
4. Karim, M.R.; Naser, J. Progress in Numerical Modelling of Packed Bed Biomass Combustion. In Proceedings of the 19th Australasian Fluid Mechanics Conference, Melbourne, Australia, 8–11 December 2014.
5. Khodaei, H.; Al-Abdeli, Y.M.; Guzzomi, F.; Yeoh, G.H. An overview of processes and considerations in the modelling of fixed-bed biomass combustion. *Energy* **2015**, *88*, 946–972. [CrossRef]
6. Yang, L.; Liu, F.; Song, Z.; Liu, K.; Saito, K. 3D numerical study of multiphase counter-current flow within a packed bed for post combustion carbon dioxide capture. *Energies* **2018**, *11*, 1441. [CrossRef]
7. Eskilsson, D.; Rönnbäck, M.; Samuelsson, J.; Tullin, C. Optimisation of efficiency and emissions in pellet burners. *Biomass Bioenergy* **2004**, *27*, 541–546. [CrossRef]
8. Porteiro, J.; Collazo, J.; Patiño, D.; Granada, E.; Gonzalez, J.C.M.; Míguez, J.L. Numerical modeling of a biomass pellet domestic boiler. *Energy Fuels* **2009**, *23*, 1067–1075. [CrossRef]
9. Kær, S.K. Numerical modelling of a straw-fired grate boiler. *Fuel* **2004**, *83*, 1183–1190. [CrossRef]
10. Yin, C.; Rosendahl, L.; Kær, S.K.; Clausen, S.; Hvid, S.L.; Hiller, T. Mathematical modeling and experimental study of biomass combustion in a thermal 108 MW grate-fired boiler. *Energy Fuels* **2008**, *22*, 1380–1390. [CrossRef]
11. Zhou, H.; Jensen, A.D.; Glarborg, P.; Jensen, P.A.; Kavaliauskas, A. Numerical modeling of straw combustion in a fixed bed. *Fuel* **2005**, *84*, 389–403. [CrossRef]
12. Cooper, J.; Hallett, W.L.H. A numerical model for packed-bed combustion of char particles. *Chem. Eng. Sci.* **2000**, *55*, 4451–4460. [CrossRef]
13. Thunman, H.; Leckner, B. Co-current and counter-current fixed bed combustion of biofuel-A comparison. *Fuel* **2003**, *82*, 275–283. [CrossRef]

14. Yang, Y.B.; Goh, Y.R.; Zakaria, R.; Nasserzadeh, V.; Swithenbank, J. Mathematical modelling of MSW incineration on a travelling bed. *Waste Manag.* **2002**, *22*, 369–380. [CrossRef]
15. Collazo, J.; Porteiro, J.; Patiño, D.; Granada, E. Numerical modeling of the combustion of densified wood under fixed-bed conditions. *Fuel* **2012**, *93*, 149–159. [CrossRef]
16. Gómez, M.A.; Porteiro, J.; Patiño, D.; Míguez, J.L. CFD modelling of thermal conversion and packed bed compaction in biomass combustion. *Fuel* **2014**, *117*, 716–732. [CrossRef]
17. Yang, Y.B.; Ryu, C.; Khor, A.; Sharifi, V.N.; Swithenbank, J. Fuel size effect on pinewood combustion in a packed bed. *Fuel* **2005**, *84*, 2026–2038. [CrossRef]
18. Thunman, H.; Leckner, B.; Niklasson, F.; Johnsson, F. Combustion of wood particles—A particle model for Eulerian calculations. *Combust. Flame* **2002**, *129*, 30–46. [CrossRef]
19. Mehrabian, R.; Scharler, R.; Obernberger, I. Effects of pyrolysis conditions on the heating rate in biomass particles and applicability of TGA kinetic parameters in particle thermal conversion modelling. *Fuel* **2012**, *93*, 567–575. [CrossRef]
20. Mehrabian, R.; Zahirovic, S.; Scharler, R.; Obernberger, I.; Kleditzsch, S.; Wirtz, S.; Scherer, V.; Lu, H.; Baxter, L.L. A CFD model for thermal conversion of thermally thick biomass particles. *Fuel Process. Technol.* **2012**, *95*, 96–108. [CrossRef]
21. Ström, H.; Thunman, H. CFD simulations of biofuel bed conversion: A submodel for the drying and devolatilization of thermally thick wood particles. *Combust. Flame* **2013**, *160*, 417–431. [CrossRef]
22. Gómez, M.A.; Porteiro, J.; Patiño, D.; Míguez, J.L. Fast-solving thermally thick model of biomass particles embedded in a CFD code for the simulation of fixed-bed burners. *Energy Convers. Manag.* **2015**, *105*, 30–44. [CrossRef]
23. Gómez, M.A.; Porteiro, J.; De la Cuesta, D.; Patiño, D.; Míguez, J.L. Dynamic simulation of a biomass domestic boiler under thermally thick considerations. *Energy Convers. Manag.* **2017**, *140*, 260–272. [CrossRef]
24. Peters, B.; Bruch, C. Drying and pyrolysis of wood particles: Experiments and simulation. *J. Anal. Appl. Pyrolysis* **2003**, *70*, 233–250. [CrossRef]
25. Wiese, J.; Wissing, F.; Höhner, D.; Wirtz, S.; Scherer, V.; Ley, U.; Behr, H.M. DEM/CFD modeling of the fuel conversion in a pellet stove. *Fuel Process. Technol.* **2016**, *152*, 223–239. [CrossRef]
26. Bhuiyan, A.A.; Naser, J. Computational modelling of co-firing of biomass with coal under oxy-fuel condition in a small scale furnace. *Fuel* **2015**, *143*, 455–466. [CrossRef]
27. Bhuiyan, A.A.; Naser, J. Numerical modelling of oxy fuel combustion, the effect of radiative and convective heat transfer and burnout. *Fuel* **2015**, *139*, 268–284. [CrossRef]
28. Yu, Z.; Ma, X.; Liao, Y. Mathematical modeling of combustion in a grate-fired boiler burning straw and effect of operating conditions under air- and oxygen-enriched atmospheres. *Renew. Energy* **2010**, *35*, 895–903. [CrossRef]
29. Nimmo, W.; Daood, S.S.; Gibbs, B.M. The effect of O2enrichment on NOx formation in biomass co-fired pulverised coal combustion. *Fuel* **2010**, *89*, 2945–2952. [CrossRef]
30. Bryden, K.M.; Ragland, K.W. Numerical modeling of a deep, fixed bed combustor. *Energy Fuels* **1996**, *10*, 269–275. [CrossRef]
31. Hagge, M.J.; Bryden, K.M. Modeling the impact of shrinkage on the pyrolysis of dry biomass. *Chem. Eng. Sci.* **2002**, *57*, 2811–2823. [CrossRef]
32. Gómez, M.A.; Comesaña, R.; Feijoo, M.A.Á.; Eguía, P. Simulation of the effect of water temperature on domestic biomass boiler performance. *Energies* **2012**, *5*, 1044–1061.
33. Thunman, H.; Niklasson, F.; Johnsson, F.; Leckner, B. Composition of volatile gases and thermochemical properties of wood for modeling of fixed or fluidized beds. *Energy Fuels* **2001**, *15*, 1488–1497. [CrossRef]
34. Gómez, M.A.; Porteiro, J.; Patiño, D.; Míguez, J.L. Eulerian CFD modelling for biomass combustion. *Transient simulation of an underfeed pellet boiler. Energy Convers. Manag.* **2015**, *101*, 666–680. [CrossRef]
35. Gómez, M.A.; Porteiro, J.; de la Cuesta, D.; Patiño, D.; Míguez, J.L. Numerical simulation of the combustion process of a pellet-drop-feed boiler. *Fuel* **2016**, *184*, 987–999. [CrossRef]
36. Andersen, J.; Jensen, P.A.; Meyer, K.E.; Hvid, S.L.; Glarborg, P. Experimental and numerical investigation of gas-phase freeboard combustion. *Part 1: Main combustion process. Energy Fuels* **2009**, *23*, 5773–5782.
37. Jones, W.P.; Lindstedt, R.P. Global reaction schemes for hydrocarbon combustion. *Combust. Flame* **1988**, *73*, 233–249. [CrossRef]

38. Brink, A.; Kilpinen, P.; Hupa, M. A simplified kinetic rate expression for describing the oxidation of volatile fuel-N in biomass combustion. *Energy Fuels* **2001**, *15*, 1094–1099. [CrossRef]
39. Wakao, N.; Kaguei, S.; Funazkri, T. Effect of fluid dispersion coefficients on particle-to-fluid heat transfer coefficients in packed beds. *Correlation of nusselt numbers. Chem. Eng. Sci.* **1979**, *34*, 325–336. [CrossRef]
40. Gómez, M.A.; Patiño, D.; Comesaña, R.; Porteiro, J.; Álvarez Feijoo, M.A.; Míguez, J.L. CFD simulation of a solar radiation absorber. *Int. J. Heat Mass Transf.* **2013**, *57*, 231–240. [CrossRef]
41. Shin, D.; Choi, S. The combustion of simulated waste particles in a fixed bed. *Combust. Flame* **2000**, *121*, 167–180. [CrossRef]



© 2018 by the authors. Licensee MDPI, Basel, Switzerland. This article is an open access article distributed under the terms and conditions of the Creative Commons Attribution (CC BY) license (http://creativecommons.org/licenses/by/4.0/).